

Key Amino Acid Associated with Acephate Detoxification by *Cydia pomonella* Carboxylesterase Based on Molecular Dynamics with Alanine Scanning and Site-Directed Mutagenesis

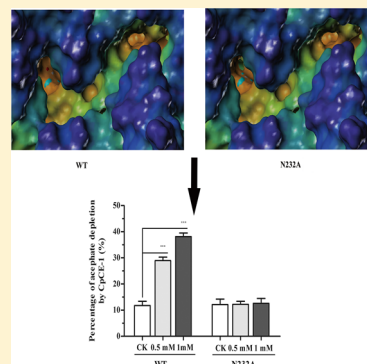
Xue Qing Yang,^{†,‡} Ji Yuan Liu,^{†,‡} Xian Chun Li,[‡] Mao Hua Chen,[§] and Ya Lin Zhang^{*,†}

[†]Key Laboratory of Plant Protection Resources & Pest Management of Ministry of Education and [§]Key Laboratory of Crop Pest Integrated Pest Management on the Loess Plateau of Ministry of Agriculture, Northwest A & F University, Yangling 712100, Shaanxi, China

[‡]Department of Entomology, The University of Arizona, Tucson, Arizona 85721, United States

Supporting Information

ABSTRACT: Insecticide-detoxifying carboxylesterase (CE) gene CpCE-1 was cloned from *Cydia pomonella*. Molecular dynamics (MD) simulation and computational alanine scanning (CAS) indicate that Asn 232 in CpCE-1 constitutes an approximate binding hot-spot with a binding free energy difference ($\Delta\Delta G_{\text{bind}}$) value of 3.66 kcal/mol. The catalytic efficiency (kcat/km) of N232A declined dramatically, and the half inhibitory concentrations (IC_{50}) value increased by more than 230-fold. Metabolism assay in vitro reveals that the acephate could be metabolized by wild CpCE-1, whereas N232A mutation is unable to metabolize the acephate, which suggests that the hot-spot Asn 232 is a crucial residue for acephate metabolism. Mutation detection suggests that low frequency of Asn 232 replacement occurred in Europe field strains. Our MD, CAS, site-directed mutagenesis, and metabolism studies introduce a new amino acid residue Asn 232 involved in the metabolism of the acephate with CpCE-1, and this method is reliable in insecticide resistance mechanism research and prediction of key amino acids in a protein which is associated with specific physiological and biochemical functions.



1. INTRODUCTION

Carboxylesterases (CEs) are enzymes belonging to the α/β hydrolase fold superfamily that hydrolyzes numerous endogenous and exogenous compounds containing a functional group such as a carboxylic acid ester, amide, and thioester and irreversible inhibition by organophosphates (OPs). In insects, CEs play a key role in the detoxification of many insecticides, including OP insecticides.^{1,2} The mechanisms of OPs are detoxified by forming irreversible complexes in a process known as a “scavenging mechanism”.²

The codling moth, *Cydia pomonella* (L.) (Lepidoptera: Tortricidae), is an economically important pest of pome fruits and walnuts in almost all areas where these crops are cultivated.³ Although environmentally compatible methods such as mating disruption⁴ and attract-and-kill strategies⁵ have been used against codling moth,⁶ chemical insecticides are often the most effective and inexpensive method for managing codling moth and are traditional used for its control.⁶ OPs are the insecticides most extensively used in crop protection over the past four decades.⁷ However, the increasing frequency and extensive use of OPs have led to serious resistance problems in several countries since the early 1990s.^{8–11} Acephate, an OPs insecticide, is one of the most commonly used insecticides for codling moth control in China.

In the codling moth, extensive studies show that increased⁷ or decreased^{10,12} CEs activity is observed using a model

substrate in OPs resistant populations compared to sensitive strains. This may be due to modified affinities to carboxylesterase substrates and increased metabolism of insecticides.^{7,13} However, limited studies have been focused on CEs in codling moth, and specific CEs genes and proteins involved in insecticide detoxification in codling moth have not yet been defined. Although the literature indicates that modified CEs may be involved in OPs detoxification,^{7,10,12,13} the structural basis and molecular biochemistry of the specific CEs mutation complex for OPs in the codling moth are poorly understood.

To date, specific point mutations in carboxylesterase have been documented in many species.^{14,15} Mutations in a carboxylesterase associated with increased activity toward OPs and decreased activity toward a generic substrate such as naphthyl acetate have been proposed,^{14,15} and many species may be affected by similar mechanisms and mutations.¹⁴ Substitution of A/G137 by aspartate (A/G121D, denoted as A121D in this paper) and W251 by leucine/serine (W251L/S, denoted as W233L in this paper) have been found in OP-resistant strain in Dipterans.¹⁴ The same amino acid residues corresponding to an Ala/Gly¹³⁷ → Asp and Trp²⁵¹ → Leu/Ser mutation in other insects were found to have significantly reduced carboxylesterase activity and conferred OP hydrolase

Received: March 13, 2014

Published: April 21, 2014



activities.¹⁶ To our knowledge, insecticides resistance has not been reported in China. The specific point mutations in *C. pomonella* CEs associated with detoxification of OPs have not been reported previously.

The recently resolved crystal structure of mammalian carboxylesterase hCE1 and rCE,^{17,18} *Bacillus subtilis* carboxylesterase (Pnb CE),¹⁹ *Aspergillus niger* EstA,²⁰ belong to the same α/β hydrolase superfamily. They share three similar domains: a canonical Ser/Glu/His catalytic triad, an α/β domain, and a regulatory domain. Interestingly, the catalytic triad is located at the base of a deep catalytic cavity.^{2,20} Even so, there are some differences. HCE1 has two substrate binding pockets: one is small and rigid and the other is large and flexible.²¹ Two 16-amino acid loops (355–370 and 450–466) are disordered and not observed in hCE1 but exist in a rabbit rCE.^{17,21} In addition, differences on the N-linked glycosylation chain, exit form are observed.² However, insect carboxylesterase structure is less known for the ligand OP insecticides, only the *Drosophila melanogaster* carboxyl/cholinesterase (DmAChE) structure has been reported.¹

In human butyrylcholinesterase (BChE), molecular modeling, molecular docking, and MD simulations have been performed to study cocaine binding with BchE.²² However, the method that using MD with alanine scanning and site-directed mutagenesis to investigate crucial amino acids in binding and detoxification of xenobiotics has not been used in insect. Thus, the method used here can provide evidence to investigate the molecular mechanism of organophosphates metabolism related to a CEs mutation in insects. In this study, we cloned a new carboxylesterase gene, *CpCE-1*, from *C. pomonella*. The structural model of CpCE-1–acephate complex was constructed by homology modeling. The MD simulation and computational alanine scanning (CAS) were conducted to predict the key amino acids associated with binding and detoxification of acephate. Site-directed mutagenesis, enzyme kinetics, and liquid chromatography were performed to verify the simulations. Our studies provide the first structural view of CpCE-1, introduce a new amino acid residue Asn 232 involved in the metabolism of the acephate with CpCE-1, and also deepen our understanding of the mechanism of detoxification of acephate. Our structural model and strategies provide clues to guide rational enzyme redesign to overcome acephate resistance and also provide evidence for designing novel pesticides. This study is reliable in insecticide resistance mechanism research and prediction of key amino acids in a protein which associated with specific physiological and biochemical functions.

2. MATERIALS AND METHODS

2.1. Insects. *C. pomonella* larvae were collected from abandoned apple orchards from Wuwei city (Gansu Province, China), a nonmanaged codling moth affected area, and were reared on flesh apples in the laboratory at a 16:8 h light:dark photoperiod, $25 \pm 1^\circ\text{C}$, and $60 \pm 5\%$ relative humidity without exposure to any insecticide.

2.2. Carboxylesterase CpCE-1 isolation. Total RNA was extracted from *C. pomonella* adults using the RNAiso Plus Kit (Takara, Dalian, China) according to the manufacturer's instructions and then treated with DNase I (Fermentas International Inc., Burlington, Canada) to eliminate DNA contamination. The first strand cDNA for conserved region amplification was synthesized using the First Strand cDNA Synthesis Kit (Fermentas) according to the procedure

recommended. For 3'-rapid amplification of cDNA ends (3'RACE), the first strand cDNA was synthesized from 1 μg of total RNA using the SMART RACE cDNA Amplification Kit (Clontech, Dalian, China) as described by the manufacturer. For 5'-rapid amplification of cDNA ends (5'RACE), single-stranded cDNA was synthesized from 1 μg of total RNA by 5'-Full RACE Kit (Takara) according to the procedure recommended.

Two degenerate sense primers CR-F1 and CR-F2 (Supporting Information Table S1) and one degenerate antisense primer CR-R (Table S1) for conserved region amplification were designed based on the consensus amino acid domain of insects CEs deposited in the NCBI database using CODEHOP.²³ The PCR was conducted in a C1000 Thermal Cycle (Biorad, USA), and a 25 μL reaction mixture containing 2.5 μL buffer, 2 μL dNTP, 0.5 μL of each primer, 20 ng cDNA, and 2 U of *Taq* polymerase (Takara) following reaction cycles of 94 °C for 3 min, 35 cycles of 30 s at 94 °C, 30 s at 55 °C, and 70 s at 72 °C, followed by 72 °C for 10 min. The target gene fragment was amplified by seminested PCR using CR-F2 and CR-R as the primer pair. The PCR product of expected size (1057 bp) was gel purified and cloned into the pMD-19 T vector (Takara) and positive clones were sequenced by Shanghai Sunny Biotech Co., Ltd.

To obtain 3- and 5-flanking sequences, gene-specific primers (GSPs) (Supporting Information Table S1) were designed based on obtained partial cDNA sequences. For 3'RACE, a homopolymeric tail was then added to the 3'-end of purified cDNA using an antisense 3'-RACE CDS Primer A, and tailed cDNA was amplified by seminested PCR using GSP1 and 10 X Universal Primer Mix (UPM) as primer pairs for the first round PCR reaction and GSP2 combination with UPM for the second round PCR amplification. For 5'RACE, PCR was carried out by nested PCR using GSP3/GSP4 and Outer/Inner primer as the primer pair. For the 3' and 5'RACE, PCR reaction conditions were the same except for the annealing temperature. The PCR product was cloned and sequenced as described above. Based on sequencing results of the 3' and 5'RACE products, specific primers WF and WS (Table S1) were designed for the full-length of CE cDNA amplification. The full-length cDNA sequence was subjected to ORF finder²⁴ for open reading frame (ORF) searching. The whole ORF nucleotide sequence containing the *Bam*H I and *Hind*III restriction sites was amplified using high-fidelity *Ex Taq* polymerase (Takara) using primers pairs ORF-F and ORF-R (Table S1). The PCR was performed at 94 °C for 3 min, followed by 35 cycles of 94 °C for 30 s, 60 °C for 30 s, and 72 °C for 2 min, with a final extension at 72 °C for 7 min.

2.3. Sequence Analysis. The deduced amino acid sequence of CpCE-1 was aligned with 12 insect CEs which were highly homologous to CpCE-1 using the ClustalX. An unrooted tree was constructed using MEGA4²⁵ under the Poisson-correction model. A total of 24 insect CEs were downloaded from GenBank including Diptera, Hymenoptera, Coleoptera, and Lepidoptera. The presence of a signal peptide was predicted using the SignalP 3.0.²⁶ To predict the presence and location of GPI anchor sites, the GPI-anchor Predictor PredGPI²⁷ was used. Asn-type glycosylation sites were predicted using NetOglyc.²⁸

2.4. Structural Modeling of CpCE-1. The 3D molecular model of the CpCE-1 was built with the Modeler 9.10.²⁹ We selected the CpCE-1 sequence as a probe to search for a PDB95 database that contains nonredundant PDB sequences at

95% sequence identity. According to the crystallographic R-factor, and overall sequential and structural identity, the best template was picked. The sequence alignment between the CpCE-1 sequence and the best template was generated by Align2D, and also identified by ClustalX with the Blosum scoring function.³⁰ The best alignment was selected according to both alignment scores.

Once a target–template alignment was constructed, 100 3D models of the CpCE-1 were calculated automatically with the optimization and refinement protocol used by the automodel of Modeler. Each model was first optimized using the variable target function method (VTFM) with conjugate gradients (CG). This was then refined using MD with simulated annealing (SA). We also used the loopmodel class in Modeler to refine the conformation of the loop between residues. We employed the GA341 and discrete optimized protein energy (DOPE) scores to measure the relative stability of the CpCE-1 conformation. We selected lowest one based on DOPE energy as the credible structure of CpCE-1. Using MolProbity, we generated the Protein Main-Chain dihedral Ramachandran map to identify the rationality of the stereo chemical for the structure.³¹

2.5. Construct the Model of CpCE-1–Acephate Complex. The CpCE-1–acephate complex was constructed by docking simulation using GOLD 5.1.^{32,33} The chemical structure of the acephate was derived from Pubchem.³⁴ Mercury 3.0 software³⁵ was used to add hydrogens and the coordinates were saved as MOL2 files. The 3D model structure of CpCE-1 added all hydrogen atoms and defined the correct ionization and tautomeric states of residues such as Asp, Glu, and His. Serine, threonine, and tyrosine hydroxyl groups, as well as lysine NH³⁺ groups are allowed to rotate during docking. All torsion angles of the acephate molecular structure were allowed to rotate freely. ChemPLP was been set at the default scoring function. Recent studies have demonstrated that ChemPLP is superior to the other scoring functions in GOLD for pose prediction.³⁶ The preliminary docking calculations were executed to search for the docking area to define a centroid close to the center the catalytic triad (Ser200, Glu331, and His447) within a radius of 30 Å. However, we could not obtain any binding solutions with the acephate against the key catalytic residues of the CpCE-1. In order to determine possible cavities on the surface of the CpCE-1, we utilized Metapocket2.0 pocket prediction algorithm to locate the binding pocket on the surface of the CpCE-1.³⁷ After clustering the top three pockets generated by Metapocket2.0, we chose the top two pockets as our binding pocket which is located in the center of the oxyanion hole and near the catalytic triad region. When a recalculation of the acephate docking was performed with the search area set within 30 Å from the residue Ala 121 lies in the oxyanion hole, an adequate docking space was found inside the area. The binding mode which acephate molecule positioned near the residue Ala 121 ranked first. Visualization of the structures was performed by pymol 1.3r1 edu,³⁸ VMD 1.9.1,³⁹ and Maestro.⁴⁰

2.6. Molecular Dynamics. The energy minimizations and MD simulations were performed using the Amber 12 package.⁴¹ The SANDER.MPI module in the Amber 12 program was used for the minimization, heating, and density protocols. The PMEMD.CUDA module was used for the equilibration and production simulations. Root mean squared deviation (RMSD), root-mean-square fluctuations (RMSF), and hydrogen bond analyses were performed using the p traj

module of Amber 12. The structure of the CpCE-1–acephate complex was immersed in a rectangular box of explicit TIP3P water extending at least 12 Å in each direction from the solute, and Na⁺ ions were added to maintain the neutrality of the system. The GAFF⁴² and the AMI-BCC⁴³ method were employed to set the ligand's parameters and charges. The AMBER for bioorganic systems force field (ff99SB) was chosen to depict the protein parameters.⁴⁴ Before the MD simulations, the energy minimization of the complex was performed by the steepest descent method for the first 2500 steps and the conjugated gradient method for the subsequent 2500 steps to eliminate unfavorable contacts. The solvated complex was carried out slowly, heating in the NVT ensemble from 0 to 300 K in 500 and 500 ps of density equilibration with weak restraints on the complex followed by 5 ns of constant pressure with unrestrained equilibration at 300 K. The production phase was run 50 ns using the same conditions as the phase of equilibration to prevent an abrupt jump in the potential energy. Recording the coordinates every 10 ps guaranteed that the structures are uncorrelated sufficiently far apart. All equilibration and production phase MD simulations were performed in the isothermal isobaric (NPT) ensemble using a Berendsen barostat.⁴⁵ The SHAKE algorithm was used to constrain all covalent bonds involving hydrogen atoms.⁴⁶ We used a 2 fs time step and a Langevin thermostat with a collision frequency of 2 ps⁻¹ dynamics for temperature control. The temperature was kept at 300 K and the particle-mesh-Ewald (PME) method was employed to treat the long-range electrostatic interactions.⁴⁷ Periodic boundary conditions were employed. The cutoff distances for nonbonded interactions were set at 12.0 Å.

2.7. Binding Free Energy Calculation. Molecular Mechanics Poisson–Boltzmann Surface Area (MM-PBSA) is a well-established method⁴⁸ as implemented in AMBER 12 to calculate the binding free energy for the association of the CpCE-1–acephate complex. One of the most popular solvent models which based on the Poisson–Boltzmann (PB) equation was used in this study. A total of 1000 snapshots were extracted every 10 ps from the 50 ns production trajectory. In MM-PBSA, the binding free energy (ΔG_{bind}) between a ligand (L) and a receptor (R) to form a complex RL is approximated by the following equation.

$$\Delta G_{\text{bind}} = \Delta H - T\Delta S \approx \Delta E_{\text{MM}} + \Delta G_{\text{sol}} - T\Delta S \quad (1)$$

$$\Delta E_{\text{MM}} = \Delta E_{\text{int}} - \Delta E_{\text{ele}} + \Delta E_{\text{vdW}} \quad (2)$$

$$\Delta G_{\text{sol}} = \Delta G_{\text{PB}} + \Delta G_{\text{SA}} \quad (3)$$

Here, ΔE_{MM} , ΔG_{sol} , and $-T\Delta S$ are the changes of the gas phase MM energy, the solvation free energy, and the conformational entropy upon binding, respectively. ΔE_{MM} includes ΔE_{int} is the internal energy (bond, angle, and dihedral energies), ΔE_{ele} (electrostatic), and ΔE_{vdW} (van der Waals) energies. ΔG_{PB} is the sum of electrostatic solvation energy (polar contribution), and the nonelectrostatic solvation component (nonpolar contribution), ΔG_{SA} . The polar contribution is calculated using PB model, while the nonpolar contribution is estimated by the solvent accessible surface area (SASA) using the LCPO method.⁵² The values of the interior dielectric constant and the exterior dielectric constant were set to 1.0 and 80.0, respectively. The entropy contribution ($T\Delta S$) was neglected in this study since our aim was to analyze the relative energy contributions of amino acids residues in CpCE-1–acephate complex formation.

2.8. Spectrum of Free Energy Decomposition. The interactions of the inhibitor and residue, which is valuable to qualitatively describe the binding mechanisms of the acephate to the CpCE-1, were analyzed per-residue-based decomposition method⁵³ processed in Amber12.⁵⁴ The decomposition energies for each residue in the complex were further broken down into backbone, side chain, and total contributions to their decomposition energy. The binding interactions of each inhibitor–residue pair ($\Delta G_{\text{inhibitor-residue}}$) were expressed as the sum of terms by

$$\begin{aligned}\Delta G_{\text{inhibitor-residue}} = & \Delta E_{\text{int}} - T\Delta S + \Delta E_{\text{vdW}} + \Delta E_{\text{ele}} \\ & + \Delta G_{\text{PB}} + \Delta G_{\text{CAVITY}}\end{aligned}\quad (4)$$

The nonbonded van der Waals contribution (ΔE_{vdW}) and the electrostatic energy (ΔE_{ele}) in eq 4 between acephate and each CpCE-1 residue were computed by the Sander module in Amber12. ΔG_{PB} represents the electrostatic contribution to the solvation free energy calculated by PB model, with the charges taken from the Amber parameter set. The nonpolar contribution to the solvation free energy (ΔG_{CAVITY}) was obtained by an empirical model based on the corresponding SASA. The internal energy (ΔE_{int}) is zero since it is based on a single trajectory and the entropy terms ($T\Delta S$) are neglected. The PB nonpolar solvation energies are currently not decomposable. All energy components in eq 4 were calculated using the snapshots as well as the binding free energy.

2.9. Computational Alanine Scanning Mutagenesis.

Computational alanine scanning (CAS) has been shown to be an effective and reliable method and can be now applied with an accuracy of 1 kcal/mol.⁵⁵ The advantage of this method compared with experimental alanine scanning is its high speed, which makes large-scale applications to instruct the experimental site-directed mutagenesis in order to find the hot spots at binding interfaces.^{55,56} To further verify the energy contributions of key residues in the binding interface with the acephate and study the detailed mechanisms at the structural and energetic characteristics. CAS was carried out on the CpCE-1–acephate complex, the alanine mutant trajectory is initially generated from the wild type MD trajectory by truncating the side chains of the mutated residue at $C\gamma$ replacing with a hydrogen atom and setting the $C\beta$ -H direction to that of the former $C\beta-C\gamma$ ⁵⁷ and then used to recalculate various energetic contributions. The binding free energy of the alanine mutant was calculated using the MM-PBSA approach. The $\Delta\Delta G$ is defined as the difference between the mutant and wild type complexes defined as

$$\Delta\Delta G_{\text{binding}} = \Delta G_{\text{binding-mutant}} + \Delta G_{\text{binding-wild type}} \quad (5)$$

The key residues of the CpCE-1–acephate complex were chosen from the binding interface based upon the side chain energy contributing more than 0.5 kcal/mol. The same set of snapshots obtained with the wild type complex was used to calculate the $\Delta G_{\text{binding-mutant}}$ for the mutants. Positive and negative values of $\Delta\Delta G_{\text{binding}}$ indicate the unfavorable and favorable contributions, respectively.

2.10. Site-Directed Mutagenesis. Mutations were generated by the Quickchange site-directed mutagenesis kit (Stratagene, La Jolla, CA) according to the manufacturer using specific primers, and CpCE-1 ORF was inserted into pMD19-T vector (Takara) as a template. 30–35 nucleotides long sense primer and 3' complementary primer at least 40% GC rich, 78 °C Tm primers (Supporting Information Table

S2) were designed with mutation sites in the middle of the oligonucleotides. Wild (WT) and mutants (MT) were confirmed by sequencing.

2.11. Protein Expression and Purification. The WT and MT were cloned into pET32a vector (Novagen, Darmstadt, Germany) and then transformed into *Escherichia coli* BL21 (DE3) (Novagen). A single colony was cultured in 400 mL LB medium containing 100 µg/mL ampicillin, 1% Casamino acids, 17 mM KH₂PO₄, and 72 mM K₂HPO₄ by shaking (220 rpm at 37 °C) and proteins were expressed and purified as described in previous study.⁵⁸ Purified proteins were analyzed on 12% SDS-PAGE gels, followed by Coomassie brilliant blue staining. The Trx-free protein was generated by enterokinase digestion. Protein was dialyzed against Tris-HCl/CaCl₂ (25 mM/1 mM, pH 7) buffer and quantified by the Bradford method⁵⁹ using bovine serum albumin as the standard.

2.12. Enzymatic Assays and Inhibition Studies. The carboxylesterase activities were measured by using substrate α -naphthyl acetate on 96-well transparent microplates as described.⁷ Absorbance of α -naphthol formation was determined after 30 min at room temperature at 600 nm in an Infinite M200 PRO (TECAN, Switzerland) and quantified using a α -naphthol standard curve. The results were expressed in micromoles of α -NA per milligram of protein per minute. Each test was conducted in triplicate and the average was used for statistical analysis. Seven various concentrations of α -NA (0.625–40 µM) were conducted in the kinetics study. The Michaelis constants (K_m) values and V_{\max} of WT and MT were determined based on the double reciprocal Lineweaver–Burk plots method.

Inhibition assays were measured by preincubating an appropriate amount of enzyme with seven concentrations of acephate (10¹–10⁶ mM) dissolved in methanol for 10 min prior to the addition of substrate. The remaining CE activities and kinetics constants were determined as described above. All measurements were conducted in triplicate and the half inhibitory concentrations (IC_{50}) were calculated by the Trimmed Spearman-Karber method.⁶⁰ The K_i values were converted from IC_{50} using the BotDB Web server tool⁶¹ (<http://botdb.abcc.ncifcrf.gov/toxin/kiConverter.jsp>). Triphenyl phosphate (TPP), a commercial inhibitor, was conducted to investigate the inhibition on NT and N232A activity.

2.13. Acephate Hydrolysis Assay. The acephate hydrolyase activity in purified CpCE-1 was determined by incubating 18 µg WT and N232A CpCE-1 in Tris-HCl/CaCl₂ (25 mM/1 mM, pH 7.0) buffer containing 0.5 and 1 mM acephate. Control reaction was conducted with heat inactivated proteins instead of the activated proteins. After 30 min of incubation at 30 °C, the quantity of acephate remaining was determined by reverse-phase HPLC using a C18 column (Waters, USA) with 15% methanol as the mobile phase with a monitoring absorbance wavelength of 215 nm.

2.14. Detection of CpCE-1 Mutations in Field Strains. Seven strains of *C. pomonella* adult were collected in Wuwei city and six European countries, namely France, Germany, Austria, Switzerland, Belarus, and Italy. Genomic DNA from different strains of individual *C. pomonella* adults was prepared using DNeasy Tissue Kit (QIAGEN, Germany). Primers 121F/121R and 232F/232R crossing the A121, N232, and W233 regions were designed (Supporting Information Table S1). Partial amplification of the two putative mutation regions of CpCE-1 gene were performed separately in a 25 µL reaction mixture

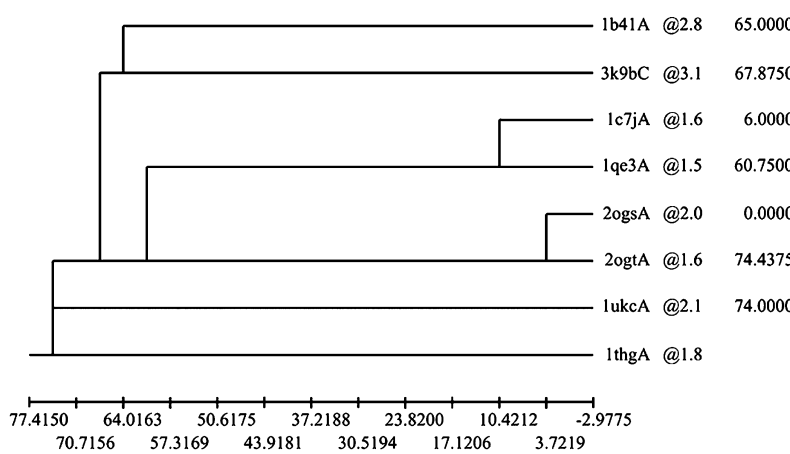
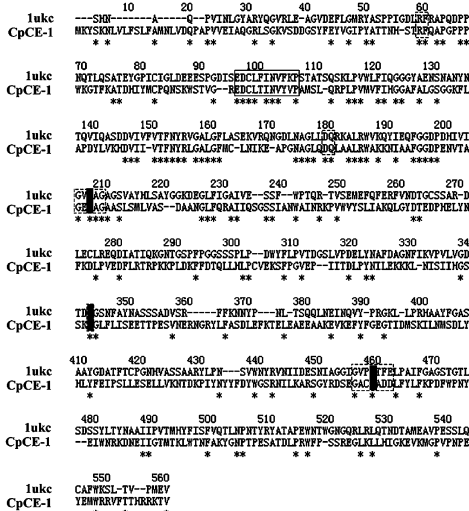
A**B**

Figure 1. Selection of the best crystal structure template for homology modeling and sequence alignments of CpCE-1 and 1ukc. (A) Weighted pair-group average clustering based on a distance matrix. 1ukc:A was selected based on a better crystallographic resolution and a higher overall sequential and structural identity to the query sequence. The last column represents the distances between this protein's cluster and those below it. The distance is basically 100%—sequence identity. The X-axis row and the second row represent the distances that each value corresponds with the position of the “+” sign on the x-axis immediately above it. (B) Comparison of CpCE-1 with *A. niger* EstA 6 (PDB ID: 1ukc:A). The carboxylesterases type-B signature 2 motif is boxed. Five catalytic domains “RF motif”, “DQ” motif, “GxSxG” version, “E” motif, and “GxxHxD/E” are outlined in dashed lines. The catalytic triad residues are shaded gray.

consisting of 3 μ L DNA template, 0.4 μ M of forward and reverse primers, 2.5 μ L 10 \times *Ex* Taq PCR Buffer, 0.2 mM of each dNTP, 1.5 Unit of *Ex* Taq polymerase (Takara) under the following cycling program: 1 cycle of 95 °C for 3 min, 35 cycles of 95 °C for 30 s, 58 °C for 30 s, 72 °C for 40 s, and a final extension at 72 °C for 7 min. The amplified PCR products were sequenced.

3. RESULTS

3.1. Homology Modeling and Constructing the Model of the CpCE-1–Acephate Complex. In order to obtain the best 3D model of CpCE-1 whose structure conserves the X-ray structure naturally, we finally selected the crystal structure of *A. niger* EstA (PDB ID: 1ukc:A) as the best crystal structure template for our homology modeling work (Figure 1A). The CpCE-1 shares 38% amino acid sequence identity with the selected template. After 100 CpCE-1 models calculated by Modeler, the best CpCE-1 model was selected with the lowest value of DOPE assessment score. Furthermore, its 3D quality was assessed by Ramachandran plot (Figure 4). The result shows that 90.6% (492/543) of all residues were in favored (98%) regions, and 97.2% (528/543) of all residues were in allowed (>99.8%) regions. The best CpCE-1 model was also validated by Profile-3D,^{62,63} and the result indicated that 77.94% of the residues with an average 3D–1D score >0.2. The residues with an average 3D–1D score less than 0.2 were far away from the binding pocket of CpCE-1 (Supporting Information Figure S5). The Ser 200, His 447, and Glu 331 (Figure 1B) of the CpCE-1 model (Green) superimposed the catalytic Ser 210, His 440, and Glu 338 of the crystal structure *A. niger* EstA (blue) very closely with the RMSD 1.84 Å (Figure 2A). All of these indicate that this 3D model is reasonable and can be used for the subsequent docking analysis.

The structure of the 3D CpCE-1 model is composed of an 11-stranded central β sheet surrounded by 18 α helices in loops

situated between the strands. (Figure 2B). The three residues of the catalytic triad (Ser 200, Glu 331, and His 447) are located at the bottom of the catalytic gorge. The CASTp⁶⁴ program predicts that the acyl pocket consists of residues Trp 233, Phe 285, Leu 289, and Phe 400, and the oxyanion hole is composed of Gly 120, Ala 121, and Ala 201 (Supporting Information Figure S2). Five cysteine residues (Cys 81, Cys 95, Cys 158, Cys 294, and Cys 446) potentially arranged as two disulfide bridges linking residues (81–95 and 158–294), which are reported to play critical roles in folding CEs into a catalytically active conformation.⁶⁵ In addition, the CpCE-1 contains four putative Asn-type glycosylation sites (residues 54, 193, 320, and 390).

The binding model of the CpCE-1–acephate complex is shown in Figure 2C. The active site contains the catalytic triad (Ser 200, Glu 331, and His 447), and is largely composed of three subsites, including the leaving group pocket (P1 subsite), the acyl pocket (P2 subsite), and oxyanion hole. In this study, the acephate is well located in the aromatic cluster made of residues Phe 122, Phe 156, and Phe 299 in the oxyanion hole lies (Figure 2C).

3.2. Stability of the Complex MD. In order to explore the stability CpCE-1–acephate complex, we performed 50 ns that the production phase lasted MD simulation for CpCE-1–acephate complex in explicit solvent. The stability was assessed by the root-mean-square deviation (RMSD) of the backbone atoms in the CpCE-1–acephate complex and the acephate molecule alone relative to the initial structure of the heating phase. From Figure 3A, we can see that the whole complex achieves equilibrium for about 30 ns with an RMSD value around 5.13 Å, indicating the stability of the complex. It can be easily seen that the conformations of the acephate molecular in the complex began to converge after nearly 20 ns with an RMSD value which fluctuates around 1.46 Å along the production phase MD trajectory. In order to further assess the stability for the binding pocket of CpCE-1–acephate

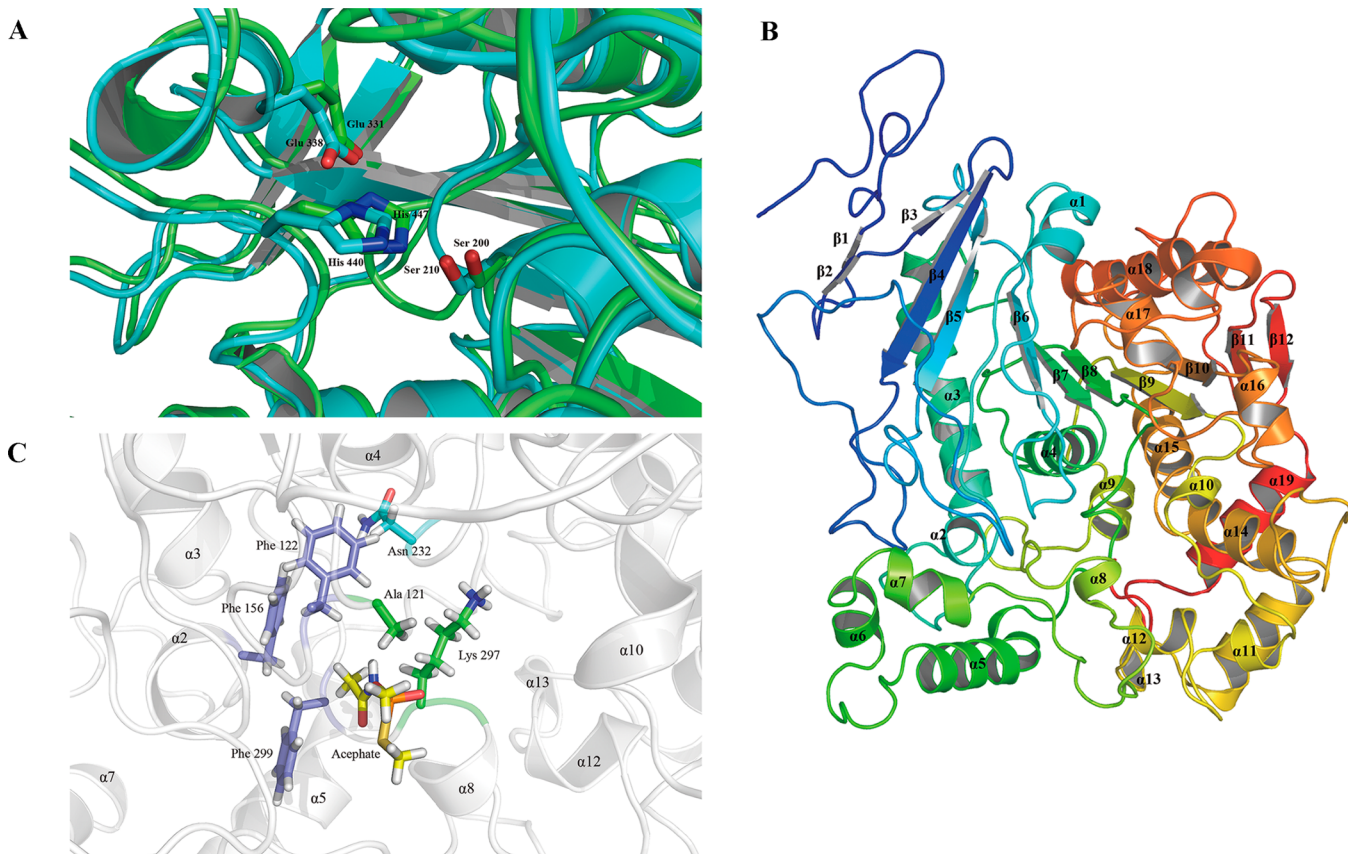


Figure 2. Structure of CpCE-1 and CpCE-1-acephate. (A) Catalytic triad of CpCE-1 and the template. The Ser 200, His447, and Glu 331 of the CpCE-1 model (green) superimpose the catalytic Ser 210, His440, and Glu338 of the crystal structure *A. niger* EstA (blue) very closely with the RMSD 1.84 Å. (B) Carton presentation of the CpCE-1 3D model using rainbow colors. Blue and red colors represent a chain trace from the N-terminus to C-terminus, respectively. (C) Binding model of the CpCE-1-acephate complex. The small molecule acephate was well located in the aromatic cluster made of residues Phe 122, Phe 156, Phe 299, and nearby the oxyanion hole constitute with Ala 121, Asn 232, and Lys 297. Phe 122, Phe 156, and Phe 299 are colored in an atom-type representation: purple (carbon), white (hydrogen). Ala 121 and Lys 297 are colored in an atom-type representation: green (carbon), white (hydrogen), and blue (nitrogen). Asn 232 is colored in atom-type representation: cyan (carbon), white (hydrogen), red (oxygen), and blue (nitrogen). Acephate is colored in atom-type representation: yellow (carbon), white (hydrogen), red (oxygen), blue (nitrogen), olive (sulfur), and orange (phosphorus).

complex,⁶⁶ the RMSD of the residues (120–124, 151, 152, 156, 232, and 294–300) within 5 Å of the acephate was also calculated (Figure 4B). It could be seen that the residues derived from the binding pocket was very stable after 30 ns with the RMSD value around 3.52 Å (Figure 3B). This reveals relatively slight changes in the structure of the acephate molecule, suggesting that the acephate molecule is equilibrated (Figure 3C) and can satisfy the requirement of our simulations.

The flexibility and the local motion in the structure of the complex were further monitored by the per-residue root-mean-square fluctuations (RMSF) from its 50 ns average positional fluctuations (Figure 3D). The average RMSF for the CpCE-1-acephate complex is 0.94 Å. The first 21 residues possessed a considerably high RMSF value due to these residues belonging to the signal peptides, while the residues Ala 121, Phe 122, Phe 156, Asn 232, Lys 297, and Phe 299 which are composed with binding interface of the CpCE-1 and are involved in interactions against the acephate molecule; they show little fluctuation even though they are all located in the loops of the CpCE-1. Although the residues 376–390 located between α 14 and α 15 fluctuate more than the other residues, this is reasonable as they all belong in the loop regions and are found far away from the binding site. This indicates that the structure

of the CpCE-1-acephate complex is equilibrated enough and quite stable along the trajectory.

3.3. Binding Free Energy. The MM-PBSA approach was employed to calculate absolute binding free energy for CpCE-acephate complex.^{49–51} The estimation of binding free energy for the CpCE-1-acephate complex is shown in Table 1. The negative total binding free energy of CpCE-1-acephate complex ($\Delta G_{\text{bind-calc}}$) is -13.87 kcal/mol. This is clearly a favorable protein–ligand complex in pure water and corresponds with the further acephate inhibition experimental values at qualitative level. Binding free energy profiles could provide a better view on which energy item has more impact in acephate binding affinity. The individual energy contribution from Table 1 shows that the van der Waals term ($\Delta E_{\text{vdW}} = -26.73$ kcal/mol) and the electrostatic energy term ($\Delta E_{\text{ele}} = -14.39$ kcal/mol) provide the major driving force for the acephate binding. Nonpolar contribution to the solvation free energy (ΔE_{CAVITY}) is -1.66 kcal/mol, which corresponds to the burial of solvent accessible surface area (SASA) and contributes slightly favorably upon binding. By contrast, the electrostatic contribution to the solvation free energy calculated by PB (ΔE_{EPB}) has the value 28.92 kcal/mol and is unfavorable for the acephate binding. To assess the reliability of the results of binding free energy, the standard errors of mean (SEM) were

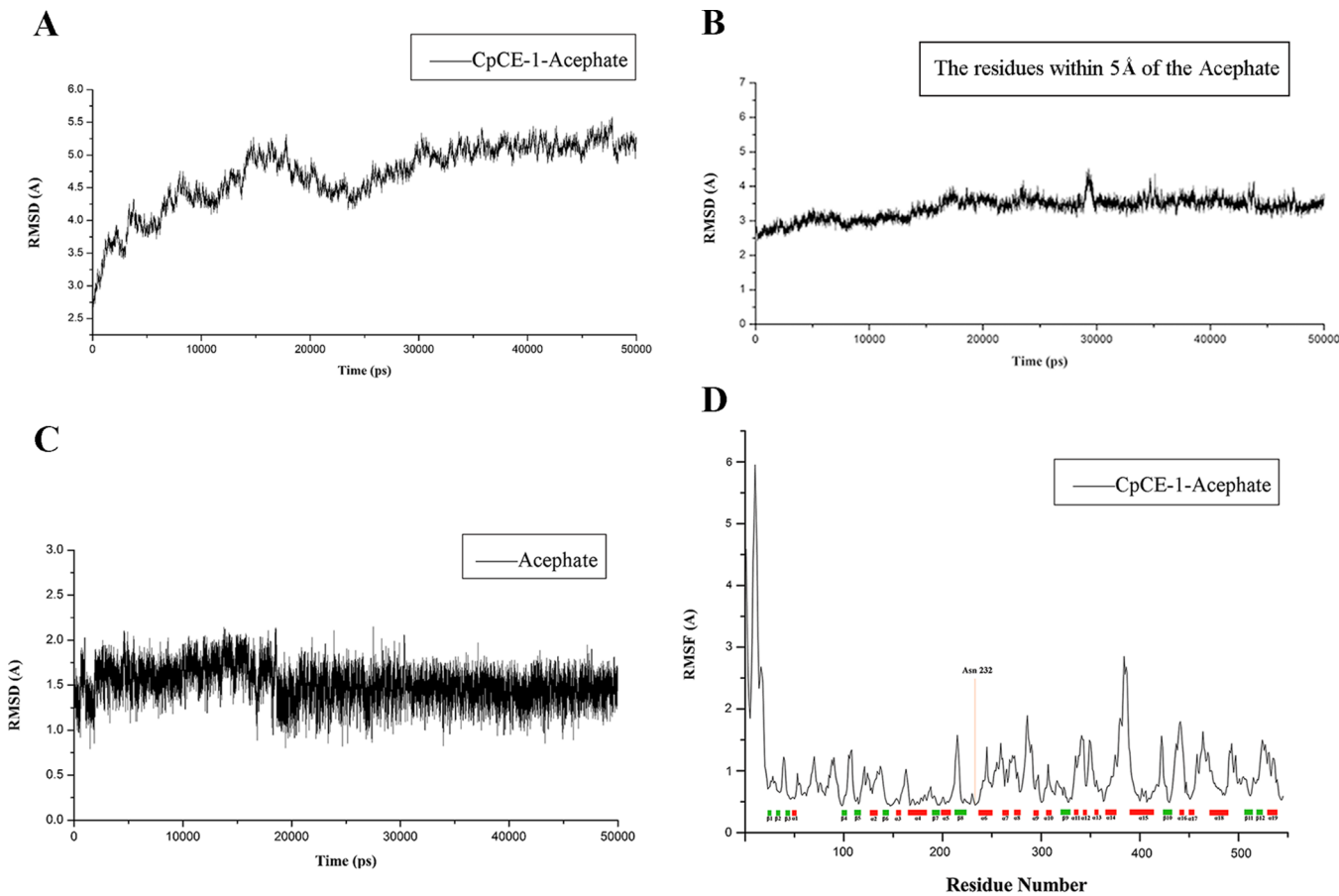


Figure 3. Stability of the complex molecular dynamics. (A) RMSD value for the whole backbone of atoms of CpCE-1–acephate complex, (B) the RMSD of the residues within 5 Å of the acephate, and (C) the acephate molecule relative to the starting structure during the equilibration phase of MD simulation. (D) Per residue RMSF of the CpCE-1–acephate complex. On the *x*-axis residues, structures that are α -helix and β -strands are indicated by the red and green bars, respectively. A red line marks the residue Asn 232.

also calculated in Table 1. The SEM for each energy item is less than 0.16 kcal/mol, indicating that the calculated binding free energy values are reliable.

3.4. Spectrum of Free Energy Decomposition for Each Residue Contribution. In order to qualitatively obtain more details of the residue energy contributions that played an important role in acephate binding, the ΔG value of binding free energy ($\Delta G_{\text{bind-calc}}$) was decomposed on a per-residue level with MM-PBSA approach. Per-residue decomposition calculates the energy contribution of single residues by summing interactions over all residues in the system. Each of these are further broken down into backbone, side chain, and total energy contributions to their decomposition energies, which were decomposed per residue into three terms: van der Waals contribution, electrostatic contribution and polar solvation contribution. The per residue contribution profile is depicted in Figure 4A and B. From Figure 4A, it can be seen that the residues of CpCE-1 in the binding interface contribute more than 0.5 kcal/mol to the total binding free energy include Ala 201, Ser 205, Asn 232 (>1 kcal/mol), Lys 297 (>1 kcal/mol), Ser 298, Phe 299 (>1 kcal/mol), and Pro 300. In contrast, Ala 121, Ala 231, and Arg 237 contribute the positive energy, and the residue Arg 237 offers unfavorable energy of more than 0.5 kcal/mol to the total binding free energy. According to Supporting Information Table S3, it is interesting to find that the dominant favorable binding free energies of those residues are mainly from van der Waals and electrostatic energies.

To reveal the binding free energy contribution of the crucial residues derived from the structural perspective, the detailed interactions between these residues and the acephate were analyzed and displayed in Supporting Information Table S3 and Figure 4C and D. The VDW item in Table S3 mostly represents the hydrophobic contacts between the molecules. The hydrophobic residues include Ala 201, Phe 299, and Pro 300, which can form the strong van der Waals interaction with the acephate. Noticeably, the backbone atoms of the residue Phe 299 contributes remarkable electrostatic energy with a high value (-5.128 kcal/mol). It is not surprising since the residue Phe 299 either forms the important hydrogen bond or hydrophobic contact. For the polar and the hydrophilic residues Ser 205, Asn 232, Lys 297, and Ser 298, the electrostatic energy is the major driving force binding the acephate. Among them, the van der Waals contributions of Asn 232 and Lys 297 are more than 1 kcal/mol. A similar trend is also shown in the interaction diagram of Figure 4D that snapshots the average conformation of the CpCE-1–acephate complex during the whole production phase. The basis of the binding pocket is composed of several hydrophobic residues including Ala 121, Phe 122, Ala 123, Phe 156, Ala 201, Ala 231, Phe 299, and Pro300, which form hydrophobic contacts around the different parts of the acephate. The residues Asn 232 and Ser 298 provide polar interaction nearby the acephate. Due to the presence of a lone pair of electrons in the amide group of Asn 232 and being closer to the acephate (2.8 Å), it contributes

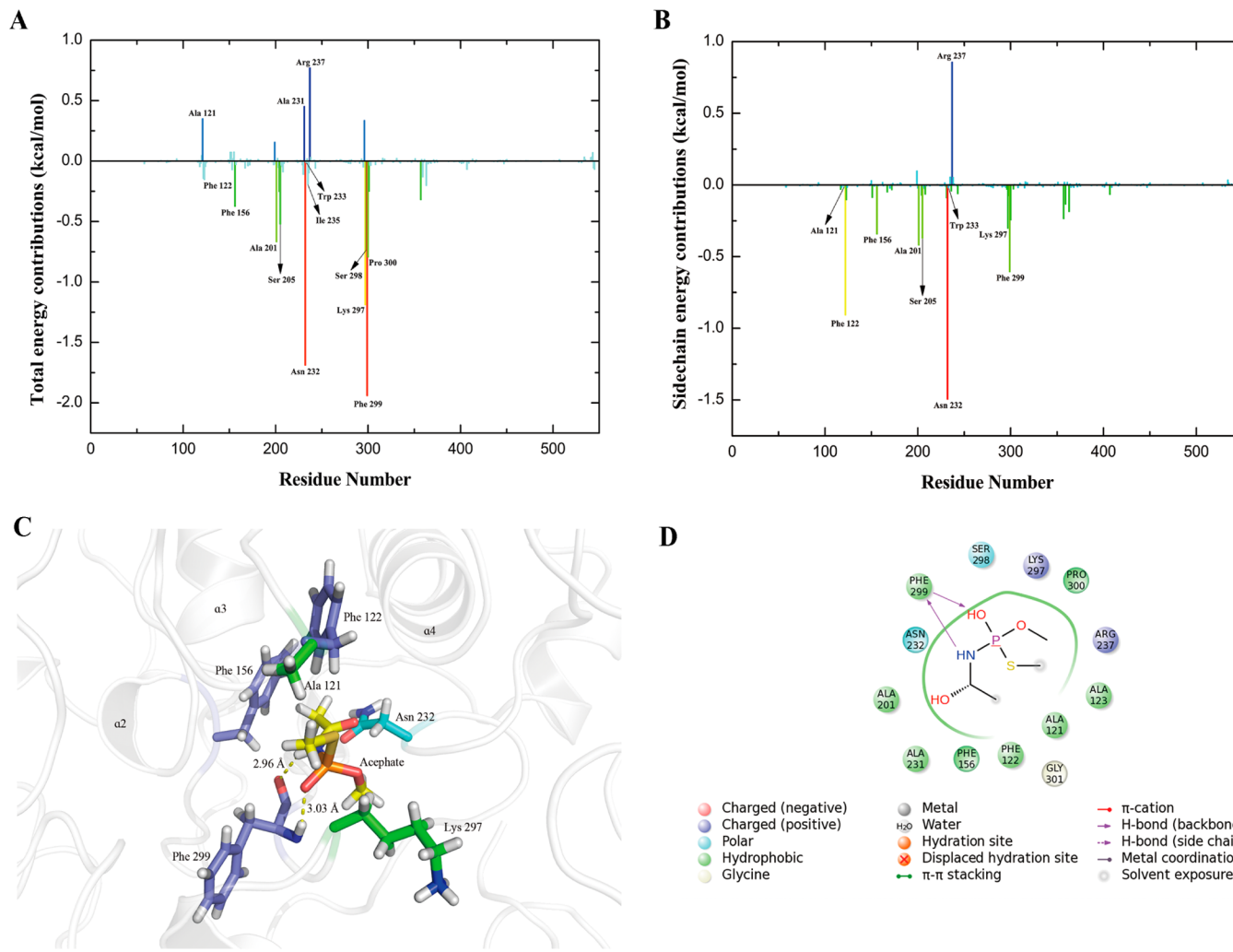


Figure 4. Residue–residue interaction spectra of the CpCE-1–acephate complex according to the MM-PBSA method. The *x*-axis denotes the residue number of the CpCE-1, and the *y*-axis denotes the interaction energy between the acephate and the CpCE-1 residues. The important residues for binding are marked by corresponding texts. (A) Total energy contributions. (B) Side chain energy contributions. (C) Average conformation of the CpCE-1–acephate complex during the whole production phase. Hydrogen bonds are depicted as dashed lines. Phe 122, Phe 156, and Phe 299 are colored in atom-type representation: purple (carbon) and white (hydrogen). Ala 121 and Lys 297 are colored in atom-type representation: green (carbon), white (hydrogen), and blue (nitrogen). Asn 232 is colored in atom-type representation: cyan (carbon), white (hydrogen), red (oxygen), and blue (nitrogen). Acephate is colored in atom-type representation: yellow (carbon), white (hydrogen), red (oxygen), blue (nitrogen), olive (sulfur), and orange (phosphorus). (D) Interaction diagram of the CpCE-1 with the acephate.

Table 1. Calculated and experimental binding free energy for the acephate binding to the WT and N232A^a

contribution	ΔE_{ele}	ΔE_{vdW}	ΔE_{EPB}	ΔE_{CAVITY}	ΔG_{gas}	ΔG_{sol}	$\Delta G_{\text{bind-calc}}$	$\Delta G_{\text{bind-exe}}$
WT	-14.39(0.16)	-26.73(0.080)	28.92(0.14)	-1.66(0.0029)	-41.12(0.16)	27.26(0.14)	-13.87(0.16)	-6.02
N232A (CAS)	-11.66(0.15)	-25.62(0.078)	28.79(0.13)	-1.71(0.0028)	-37.28(0.14)	27.07(0.13)	-10.21(0.15)	
N232A (MD)	-8.89(0.14)	-25.47(0.081)	33.45(0.15)	-1.69(0.0032)	-34.36(0.15)	31.76(0.15)	-2.60(0.15)	-2.85

^aAll values are given in kilocalories per mole, with corresponding standard errors of mean in parentheses.

Table 2. H-Bonding Interactions between the Acephate and the CpCE-1^a

DONOR	ACCEPTORH	ACCEPTOR					
			atom no.:res@atom	atom no.:res@atom	atom no.:res@atom	% occupied	distance
8649:546@O4	4617:299@H	4616:299@N	81.64	3.03 (0.17)	28.76 (10.08)	20.0 (25.5)	109
4635:299@O	8656:546@H11	8651:546@N6	62.92	2.96 (0.17)	42.58 (11.80)	3.3 (3.4)	27

^aThe percentage of simulation snapshots (saved every 10 ps) in which the H-bond was present is listed. The occupancy of H-bonds that are formed between the acephate and the CpCE-1 larger than 5% is listed.

a larger electrostatic energy and van der Waals than Ser 298. For the polar residue Lys 297, its main contribution to the

binding process does not come from the formation of polar interaction but comes from the obvious positive charge

Table 3. Theoretical and Experimental $\Delta\Delta G_{\text{bind}}^a$ Value for WT and Mutant CpCE-1–Acephate Complexes

protein	A121D	F122A	N232A	W233A	W233L	F299A	F299C	F299S
$\Delta\Delta G_{\text{bind-calc}}$		1.53	3.66	0.003		0.28		
$\Delta\Delta G_{\text{bind-expt}}^b$	0.66		3.17		1.39	0.22	-1.02	-1.30

^aAll values are given in kilocalories per mole. ^bThe binding free energy difference ($\Delta\Delta G_{\text{bind}}$) between the mutant and wild type complexes is defined as $\Delta\Delta G_{\text{bind}} = RT \ln(\text{IC}_{50} \text{ mutant}/\text{IC}_{50} \text{ wild type})$, where R is the ideal gas constant and T is the temperature in kelvin.

interaction of its side chain NH_3^+ group (Figure 4D). This can explain why it contributes an electrostatic energy of more than 2 kcal/mol to the acephate binding. To further discover the role of the key residues that stabilize the structure of the CpCE-1–acephate complex, we analyzed hydrogen bond networks between the acephate and the CpCE-1 based on the MD trajectory. The hydrogen bond interactions listed in Table 2 show that the acephate forms stable hydrogen bonds through its acyl and phosphorus group with the NH and O atom of Phe 299 backbone, exhibiting high occupancy rates of 81.64% and 62.92%, respectively, during the whole production process MD simulation. There were two hydrogen bonds between the CpCE-1 and the acephate in the CpCE-1–acephate complex. The O4 atom derived from the phosphorus group in the acephate and the NH atom of the Phe 299 backbone formed a hydrogen bond having a distance of 3.03 Å between atoms, while the O atom of Phe 299 backbone interacts with the H11 atom of the acephate acyl group with a hydrogen bond distance of 2.96 Å between atoms (Figure 4C). The distance fluctuation of these two hydrogen bonds was very small (0.17 Å), and the angle could satisfy the criteria. With this analysis, we could thus conclude that the hydrogen bonds of the residue Phe 299 greatly contributed to the binding of the acephate. These findings indicate that the acephate could be driven into the binding site by electrostatic guidance of Lys 297 that acts as a gatekeeper. The residue Asn 232 attracted the acephate to move inside the deepness of the binding site and constantly adjusted the pose of the acephate in order to form the stable hydrogen bond interactions to the backbone of the residue Phe 299, which similar to “pincers”. This clearly clarified the binding mechanism of the acephate to the CpCE-1.

3.5. Computational Alanine Scanning Mutagenesis. In order to completely mimic the site-directed mutagenesis using molecular biology technology to verify the binding hot-spot, three residues, Asn 232, Phe 122, and Phe 299 (Figure 4B) whose side chains contribute more than 0.5 kcal/mol according to the per-residue energy decomposition, were chosen for mutation to alanine by the computational alanine scanning (CAS) method.⁵⁵ Additionally, Trp 233 that has been reported to mutate to Leu in previous papers^{14,16} was also selected. The CAS results for the selected residues are given in Table 3. Mutation Asn 232 to Ala resulted in the largest change in binding free energy ($\Delta\Delta G_{\text{bind}} = 3.66$ kcal/mol). The residue Phe 122 is a null-spot with $\Delta\Delta G_{\text{bind}}$ lower than 2.0 kcal/mol. Interestingly, the residue Phe 299 contributes the largest total binding free energy for the acephate binding, a lower value of $\Delta\Delta G_{\text{bind}}$ (0.28 kcal/mol) was observed when mutated into alanine. The binding free energy does not drop dramatically when Trp 233 is mutated to alanine. Therefore, we further analyzed the critical residue Asn 232 that was successfully predicted to be a hot-spot for the binding of acephate. The binding free energies and the energy components (ΔE_{ele} , ΔE_{vdW} , ΔE_{EPB} , ΔE_{CAVITY} , and $\Delta G_{\text{bind-calc}}$) of the complex with the N232A and wild protein are also listed in Table 1. As shown in Table 1, the residue Asn 232 produces an obvious effect on

the ΔE_{ele} and $\Delta G_{\text{bind-calc}}$ but hardly influences ΔE_{vdW} , ΔE_{EPB} , and ΔE_{CAVITY} . Thus, the data indicate that the residue Asn 232 provides a favorable energy contribution mainly by dominant electrostatic interaction. Its side chain is a major contributor that plays an important role in the binding of the acephate in the hydrophobic active pocket. This is consistent with the previous analysis of binding free energy decomposition.

3.6. Verifying the Hot-Spot Asn 232 by MD. To verify the binding hot-spot Asn 232 of the CpCE-1, we employed the same method to perform the MD simulation and the binding free energy calculation for the N232A–acephate complex. The RMSD and RMSF plots showed that the N232A–acephate complex was considerably stable, and the conformations of the residues 226–239 ($\beta 8-\alpha 6$ loop) in which the Ala 232 located have little fluctuation (Figure 5A and B). This also proves that the mutation of the residue Asn 232 to alanine does not impact the global conformation of the N232A–acephate complex. As shown in Table 1, the negative total binding free energy of the N232A–acephate complex ($\Delta G_{\text{bind-calc}}$) is -2.60 kcal/mol, and the electrostatic energy term (ΔE_{ele}) is -8.89 kcal/mol, which corresponds with the results of CAS and are all in close agreement with the subsequent experiments. The average conformation of the N232A–acephate complex during the whole production phase is shown in Figure 5C. It can easily be seen that the NH atom and the O atom derived from the backbone of the residue Phe 299 cannot form a hydrogen bond network with the O4 atom and the H11 atom of the acephate respectively, having average distances of 5.6 and 4.2 Å between them which is larger than the criterion for the H–acceptor distance (3.5 Å) throughout the trajectory. Due to the absence of these hydrogen bonds (Figure 5D), the ΔE_{ele} reduced 5.5 kcal/mol can be compared with the CpCE-1–acephate complex, which then leads to a significant decrease in the binding free energy ($\Delta G_{\text{bind-calc}}$) by a value of more than 11 kcal/mol. According to the binding free energy decomposition (Supporting Information Table S4, Figure 5E and F), the residue Phe 299 makes an unfavorable 0.775 kcal/mol contribution to the binding free energy, while the electrostatic contribution derived from its backbone was only -0.678 kcal/mol and the van der Waals contribution was also below 1 kcal/mol. The mutation of the Asn 232 has little effect on the van der Waals contribution and electrostatic contribution with the residue Lys 297; however, it produces a noteworthy increase in the electrostatic contribution to the solvation free energy to the residue Lys 297 with a value of nearly 1 kcal/mol. This might make the residue Lys 297 partly accessible to the solvent and causes its total energy contribution to decrease to the lower value of -0.262 kcal/mol. The rest of the residues located in the binding interface have not shown any significant difference toward the binding free energy of the CpCE-1–acephate complex and the mutated state (Supporting Information Table S4). Moreover, the N232A mutation caused significant structural changes at the pipe-shaped core domain, which produced a spacious and stretched-inward cavity, but leaves the overall structure of the core domain intact (Figure 6).

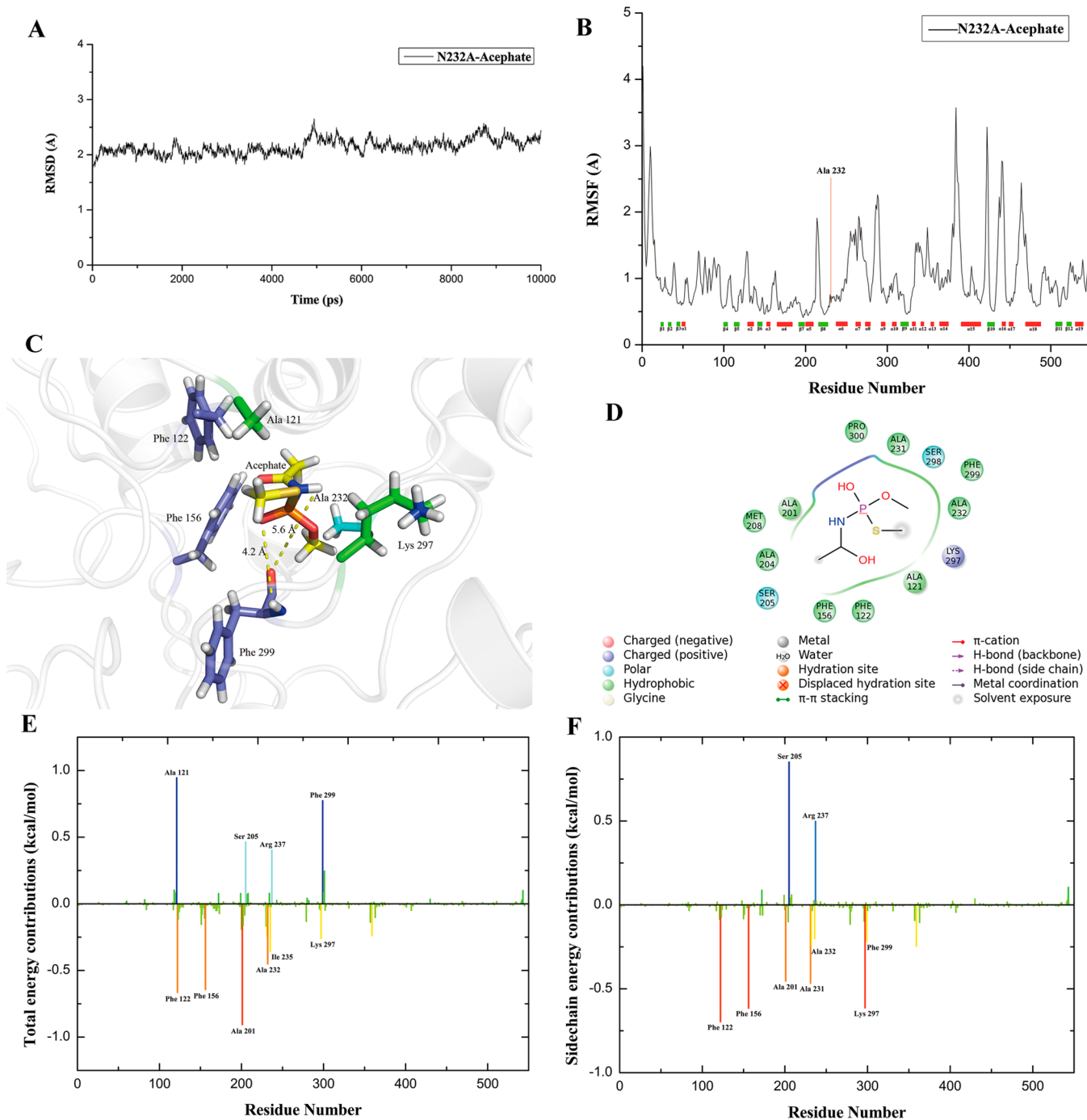


Figure 5. Verifying the hot-spot Asn 232 by molecular dynamics. (A) RMSD value for the whole backbone of atoms of N232A–acephate complex. (B) Per residue RMSF of the N232A–acephate complex. On the x -axis, residues with structures of α -helix and β -strands are indicated by the red and green bars, respectively. A red line marks the residue Ala 232. (C) Average conformation of the N232A–acephate complex during the whole production phase. The distance between the NH atom, the O atom derived from the backbone of the residue Phe 299 and the O4 atom, and the H11 atom of the acephate are depicted as dashed lines. Phe 122, Phe 156, and Phe 299 are colored in atom-type representation: purple (carbon), white (hydrogen). Ala 121 and Lys 297 are colored in atom-type representation: green (carbon), white (hydrogen), and blue (nitrogen). Ala 232 is colored in atom-type representation: cyan (carbon), white (hydrogen). Acephate is colored in atom type representation: yellow (carbon), white (hydrogen), red (oxygen), blue (nitrogen), olive (sulfur), and orange (phosphorus). (D) Interaction diagram of the N232A with the acephate. (E, F) Residue–residue interaction spectra of the N232A–acephate complex according to the MM-PBSA method. The x -axis denotes the residue number of the N232A and the y -axis denotes the interaction energy between the acephate and the N232A residues. The important residues for binding are marked by corresponding texts. (E) Total energy contributions. (F) Side chain energy contributions.

Consequently, we can speculate that the residue Asn 232 plays a most vital role in the binding of the acephate, which is consistent with the previous CAS analyses.

3.7. Site-Directed Mutagenesis and Inhibitory Kinetics of CpCE-1.

Based on computational alanine scanning, three residues, Asn 232, Phe 122, and Phe 299 whose side chain

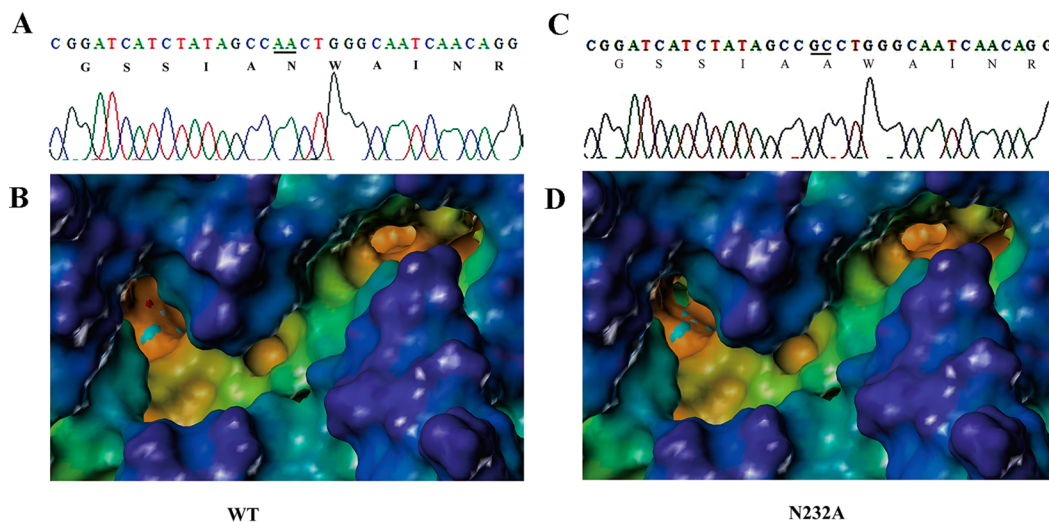


Figure 6. Sequencing map and structure of wild and N232A around residue 232. Sequencing of wild (A) and N232A (C) around residue 232. Cavity depth potential surface of the wild CpCE-1 (B) and N232A (D) around residue 232. Light red color denotes the deepest depth. Residue ASN 232 and Ala 232 represent VDW model: cyan (carbon), white (hydrogen), and red (oxygen). The cavity depth measures how deep a surface point is located inside a cavity of a molecule. The cavity depth color ramp ranges from blue (low depth values represent outside of the molecule) to light red (high depth values represent cavities deep inside the molecule).

Table 4. Kinetic Parameter and the IC₅₀ of Acephate Inhibiting WT and Mutant CpCE-1 Activities

protein	K _m (μM)	V _{max} ($\mu\text{mol min}^{-1} \text{mg}^{-1}$)	K _{cat} (s^{-1})	K _{cat} /K _m ($\text{s}^{-1} \mu\text{M}^{-1}$)	IC ₅₀ (μM)
wild	13.4 \pm 1.3	12.9 \pm 1.4	1340	100	42.108
A121D	178.7 \pm 14.1	12.8 \pm 1.7	269.9	1.51	130.257
N232A	13.4 \pm 1.6	13.3 \pm 0.9	240.1	17.91	>10 000
W233L	4.5 \pm 0.3	0.764 \pm 0.1	7.826	1.74	321.228
F299A	10.9 \pm 1.1	1.4 \pm 0.1	15.5	1.42	28.656
F299C	20.3 \pm 2.3	0.7 \pm 0.03	12.3	0.61	7.5477
F299S	12.1 \pm 1.4	3.2 \pm 0.2	56.1	4.64	5.351

energy contributes more than 0.5 kcal/mol, were selected for site-directed mutagenesis to alanine. In addition, F299C and F299S mutants were created. Two amino acid residues, Ala121 and Trp233, which were previously reported to be involved in malathion resistance in other species^{14,16} were also investigated. Our goal was to identify any mutation that significantly affected the combination of acephate to the protein.

We characterized the effect of the mutations on substrate α -NA catalysis. Kinetic parameter K_m and V_{max} were also determined by using a double reciprocal Lineweaver–Burk plot method. As shown in Table 4, the A121D mutant exhibited the highest binding affinity (K_m) toward α -NA substrate, the K_m values of the WT enzyme and N232A were almost same, but the W233L showed a lower K_m than WT, A121D, and N232A. The WT enzyme exhibited the highest catalytic efficiency (k_{cat}/K_m) toward α -NA substrate, with the k_{cat}/K_m of 100 $\text{s}^{-1} \mu\text{M}^{-1}$. This appeared to be a 5.6–165-fold decrease for the mutants compared to the WT protein. The observed decreases on k_{cat}/K_m for A121D and W233L mutations are similar to previous research.^{15,67} Interestingly, the catalytic efficiency of N232A also declined to 17.91 $\text{s}^{-1} \mu\text{M}^{-1}$. Moreover, A121D and W233L caused a significant catalytic efficiency decrease (Table 4).

The IC₅₀ of WT and MT proteins were measured (Table 4) to further investigate the effect of acephate on CE activities. The WT protein exhibited IC₅₀ of 42.108 μM for acephate. Surprisingly, N232A showed weak inhibition by acephate, with an IC₅₀ value higher than 10 mM. The IC₅₀ of acephate against

Ala121D and W233L were 3.09- and 7.63-fold higher than that observed for WT. However, the IC₅₀ of acephate against F299A, F299C, and F299S decreased dramatically, only being 0.68-, 0.18-, and 0.13-fold of WT, respectively.

The experimental $\Delta\Delta G_{\text{bind}}$ ($\Delta G_{\text{bind-exp}}$) values for both WT and mutants were calculated (Table 3). The results show a decreased $\Delta\Delta G_{\text{bind-exp}}$ value, being -1.02 and -1.30 kcal/mol for F299C and F299S, respectively. For F299A, the value is 0.22 kcal/mol. Moreover, A121D and W233L mutations exhibited 0.66 and 1.39 kcal/mol $\Delta\Delta G_{\text{bind-exp}}$ values. A huge increase of binding free energy was observed for the N232A mutant; the wild type possessed -6.02 kcal/mol binding free energy for acephate (Table 1), but the N232A variant exhibited only -2.85 kcal/mol of binding free energy by acephate. With a $\Delta\Delta G_{\text{bind-exp}}$ value of 3.17 kcal/mol (Table 3), this phenomenon is consistent with the results of the simulation above. This result indicates that the N232A mutation is unfavorable for binding the acephate.

The inhibition assay using inhibitor TPP showed that no inhibition of N232A mutant enzyme activity was observed, whereas it exhibited a high inhibition activity (nearly 60%) by preincubating the wild type enzyme with 1 mM TPP (Supporting Information Figure S6) and showed an IC₅₀ of 0.28 mM. The IC₅₀ value of TPP exhibited to WT CpCE-1 in this study is in good agreement with the value in *Aphis gossypii*⁶⁸ which are both on the same order of magnitude (mM). This result suggests that the N232A mutation is unfavorable for binding inhibitor TPP and could also confirms

why acephate exhibited dramatic changes of ΔG_{bind} for the N232A mutation.

3.8. Acephate Hydrolysis. The lower binding affinity of acephate with the N232A mutant (higher IC_{50} value) does not mean that the catalytic activity of the N232A mutant against the acephate is lower, so the metabolic activity of the WT and the N232A mutant against the acephate was further determined by HPLC. The purified WT and N232A CpCE-1 were incubated with acephate to investigate their abilities to metabolize the acephate in vitro (Figure 7). WT enzyme was able to

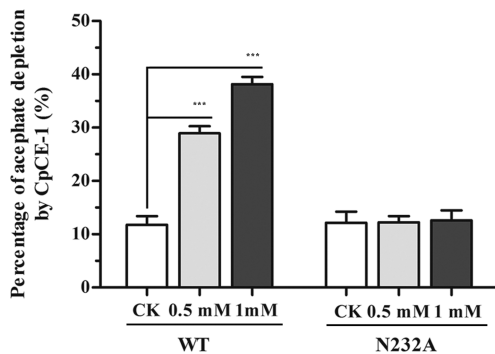


Figure 7. Metabolic activity of CpCE-1. The percentage of acephate cleared by 18 μg WT and N232A CpCE-1 at 30 °C for 30 min is indicated by pillar height. Heat-inactivated proteins were used as control. Error bars represent SD ($n = 3$). Asterisks on the error bars indicate the significant differences by student's *t*-test. (***) $P \leq 0.001$.

metabolize the acephate during the 30 min incubation. The respective proportions of acephate depletion were almost 29% and 38% in the presence of 0.5 and 1 mM acephate. However, acephate was not metabolized by N232A, with no significant difference observed between the percentage of acephate depletion in the presence or in the absence of activated N232A.

3.9. Mutation Detection of CpCE-1 Sequence from Different Strains of *C. pomonella*. The putative two mutation regions of CpCE-1 with 416 bp and 393 bp were amplified from adults of different *C. pomonella* strains (Table S5). No amino acid substitutions are found at amino acid residues 121. Noteworthy, it showed 20% and 30% frequency of amino acid replacement of Asn232 by Thr or Ala in Fra and Ger strains, respectively. For amino acid residue 233, Swi strain carried one mutant with the amino acid replacement of W233L (20% frequency).

4. DISCUSSION

To date, many studies show that CE is involved in OP detoxification in codling moth.^{12,15,18–20} We are interested in the molecular mechanism of OP detoxification, especially the key residues contributing to acephate binding and detoxification. Interestingly, the N232A mutant showed a positive correlation for $\Delta\Delta G_{\text{bind}}$ between the CAS predicted value ($\Delta G_{\text{bind-calc}}$) and $\Delta G_{\text{bind-exp}}$, with $\Delta G_{\text{bind-calc}}$ increasing from -13.87 to -2.6 kcal/mol and $\Delta G_{\text{bind-exp}}$ increasing by almost 3.17 kcal/mol, and the theoretical $\Delta\Delta G_{\text{bind}}$ being 3.66 kcal/mol. These results suggest that the calculated $\Delta\Delta G_{\text{bind}}$ value is qualitatively consistent with the experimental value, with an accuracy of almost 1 kcal/mol. The same correlation was found in F299A (Table 3). This demonstrates that the CAS methods⁵⁵ used here may be used as a general method to indicate binding and explore detoxification mechanisms

associated with CE mutations and to predict the key amino acid on target proteins participating in substrate binding and interactions. In order to investigate the effect of single amino acids mutation on binding free energy and to confirm the simulation results, site-directed mutagenesis was conducted. We selected a bacterial system that is widely used for insect CEs^{15,69} to express recombinant wild and mutation proteins. Based on this, acephate metabolism assays were performed to investigate the ability of WT and N232A for hydrolysis of acephate in vitro. Notably, acephate was significantly metabolized by WT, but N232A was unable to hydrolyze acephate. The result is another evidence to confirm the role of Asn 232 in metabolism of acephate, and consisting with previous CAs and inhibition assay. Similar study has been reported by using molecular modeling, molecular docking, and MD simulations to study cocaine binding with human butyrylcholinesterase (BChE) and its mutants.⁵²

We further investigated the conformation of the binding pocket changes affected by the N232A mutation. Many of the previous studies have shown that the active and nonactive site substitution lead to a conformation change of the binding pocket which altered the interaction between the protein and inhibitor.^{70,71} In our study, the N232A mutation produces a spacious and stretched-inward cavity but does not influence the pipe-shaped core domain structure and protein-folding markedly, which is unfavorable to its binding the acephate. This may explain why weak acephate inhibition activity and unable metabolized acephate observed in our experiment. The phenomenon of the conformation change after the amino acid residue mutation observed in our study is consistent with previous works in other enzymes.^{68,70,71}

Previous studies suggested that mutations in carboxylesterase are associated with resistance to OPs in many insect species by similar mechanisms.^{14,15} A/G137D (Ala 121) and W251L/S (Trp 233) have been reported to relate with field OPs-resistant in Dipteran insects^{14,15} by increasing metabolism of OPs. N232A has not been reported to associate with insecticides resistance in any other insects. In this study, N232A mutation led to significant conformation changes at the binding pocket and with dramatic acephate $\Delta\Delta G_{\text{bind}}$. However, N232A is not compatible with previous reported mutants because N232A mutation make insects more susceptible to acephate, rather than resistant to acephate. Moreover, the 20% frequency of N232A mutation and 30% for N232T observed in European Fra and Ger strains, where OPs resistant has been reported,^{8,10} suggesting that N232A/T mutations may be no accident occurred in fields and associated with the OPs resistance reported in these areas.^{8,10} Another amino acid residue substitution, W233L mutation was found in the Swi strain, indicating that this amino acid residue replacement has developed in Swi field strain and this may be one of the reason for development of OPs resistance observed in Switzerland.¹⁰ Whether these strains are resistance strains or susceptible strains remains unknown, and the use of insecticides in these countries to control *C. pomonella* is less known. However, the detected mutation frequencies in different source of adult strains, together with the MD and site-directed mutagenesis results, suggest that N232A play an important role in development of OPs resistance and also suggest that Asn 232 is a key amino acid associated with acephate detoxification in *C. pomonella*.

In enzyme redesign engineering, using computational methods such as the CAS method used in this study, combined

with experimental data, could provide some clues to the deep understanding of the structure-dynamic-activity relationships^{55,72} and offer ways to predict and possibly overcome resistance^{73,74} and to guide rational redesign.⁵⁵ In the present study, the WT enzyme can be half inhibited by acephate (μM); however, N232A mutation results are not suited for acephate binding (weak inhibition observed). We hypothesize that poor control effects would be found in using acetyl-containing insecticides such as acephate on a resistant population where Asn 232, or other residues crucial for binding insecticides, mutated to residues promoting carboxylesterase binding with insecticides. This also can explain why some chemical controls failed for codling moth in the early 1990s in southeastern Europe,⁷⁵ which may have been due to some key amino acid residues have mutated in carboxylesterase. Meanwhile, the Arg 237 and Ser 205, whose contributions in WT and N232A for binding free energies (Figure 4B, SE and F) on protein side chains are unfavorable for acephate binding (positive value); such residues unfavorable for acephate binding should be redesigned by rational site-directed mutagenesis^{76,77} to residues more unfavorable to binding molecules in order to achieve a good control effect in the orchard. In the other direction, the enzymes containing such residues unfavorable for acephate binding could be redesigned toward the opposite direction which is beneficial for binding insecticides and used in degradation of acephate or other acetyl-contained insecticides that remain in exported fruits. For instance, the residues Asn 232, Phe 122, and Phe 299, in addition to Ala 201, Ser 205, Phe 156, and other amino acids (Figures 4B, 5E and 5F) in CpCE-1 that are favorable for acephate binding should be retained or rationally redesigned toward the direction of combining more closely with molecules in order to pursue a better effect in the future enzyme redesign engineering. Based on the predicted CpCE-1 3D structure, using structure-based drug design,⁷⁸ novel OPs pesticides could be designed and rational enzymes could be redesigned in the future.

5. CONCLUSION

This work sheds new light on the molecular mechanism of acephate (OP) metabolism related to a CEs mutation in insects. We show that the method, using MD with alanine scanning and site-directed mutagenesis, is reliable in investigation of the molecular mechanism of organophosphates metabolism related to a CEs mutation in insects. This method may be used as a general method to indicate binding and explore detoxification mechanisms associated with CEs mutation and to predict the key amino acid on target proteins participating in substrate binding and interactions in insect. Our experimental data provides support for introduction a new amino acid residue Asn 232 involved in the metabolism of the acephate with CpCE-1, and this information could be applicable to investigate the OPs-resistance mechanism, to develop pesticide-degraded engineered bacteria and for structure-based insecticide design in future.

■ ASSOCIATED CONTENT

Supporting Information

Results of sequence analyses and phylogeny. This material is available free of charge via the Internet at <http://pubs.acs.org>.

■ AUTHOR INFORMATION

Corresponding Author

*Tel./Fax: +86-29-8709-2190. E-mail: yalinzh@nwsuaf.edu.cn.

Author Contributions

¹X.Q.Y. and J.Y.L. contributed equally to this work.

Author Contributions

X.C.L. and M.H.C. conceived the project and designed the experiments. X.Q.Y. and J.Y.L. performed the experiments and wrote the paper. M.H.C. collected the codling moth samples. Y.L.Z. supervised the study and contributed reagents/materials. All authors contributed to data analysis.

Notes

The authors declare no competing financial interest.

■ ACKNOWLEDGMENTS

We thank Dr. John Richard Schrock from Emporia State University (Kansas, USA) for proofreading this manuscript before submission. We also thank Dr. Sobereva for valuable suggestion in molecular dynamics. This work was supported by the Special Fund for Agro-scientific Research in the Public Interest of China (No. 200903042-03) and National Natural Science Foundation of China (No.31071687).

■ REFERENCES

- (1) Oakeshott, J. G.; Cludianos, C.; Campbell, P. M.; Newcomb, R. D.; Russell, R. J. In *Comprehensive Molecular Insect Science-Pharmacology*; Gilbert, L. I.; Latrou, K.; Gill, S. S., Eds.; Elsevier: Oxford, 2005; Chapter 5, pp 309–381.
- (2) Yan, B. In *Encyclopedia of Drug Metabolism and Interactions*; Lyubimov, A. V., Ed.; Wiley & Sons: Hoboken, NJ, 2012; Vol. 6, Chapter 14, pp 1–34.
- (3) Rodríguez, M. A.; Marques, T.; Bosch, D.; Avilla, J. Assessment of insecticide resistance in eggs and neonate larvae of *Cydia pomonella* (Lepidoptera: Tortricidae). *Pestic. Biochem. Phys.* **2011**, *100*, 151–159.
- (4) Charmillot, P. J. Mating disruption technique to control grape and wine moths: general considerations. *IOBC. WPRS. Bull.* **1992**, *15*, 113–116.
- (5) Charmillot, P. J.; Hofer, D.; Pasquier, D. Attract and kill: a new method for control of the codling moth *Cydia pomonella*. *Entomol. Exp. Appl.* **2000**, *94*, 211–216.
- (6) Voudouris, C. C.; Sauphanor, B.; Frank, P.; Reyes, M.; Mamuris, Z.; Tsitsipis, J. A.; Vontas, J.; Margaritopoulos, J. T. Insecticide resistance status of the codling moth *Cydia pomonella* (Lepidoptera: Tortricidae) from Greece. *Pestic. Biochem. Phys.* **2011**, *100*, 229–238.
- (7) Reyes, M.; Collange, B.; Rault, M.; Casanelli, S.; Sauphanor, B. Combined detoxification mechanisms and target mutation fail to confer a high level of resistance to organophosphates in *Cydia pomonella* (L.) (Lepidoptera: Tortricidae). *Pestic. Biochem. Phys.* **2011**, *99*, 25–32.
- (8) Sauphanor, B.; Bouvier, J.; Brosse, V. Spectrum of insecticide Resistance in *Cydia pomonella* (Lepidoptera: Tortricidae) in South-eastern Franc. *J. Econ. Entomol.* **1998**, *91*, 1225–1231.
- (9) Pasquier, D.; Charmillot, P. J. Effectiveness of twelve insecticides applied topically to diapausing larvae of the codling moth, *Cydia pomonella* L. *Pest. Manag. Sci.* **2003**, *60*, 305–308.
- (10) Reyes, M.; Frank, P.; Charmillot, P. J.; Ioriatti, C.; Olivares, J.; Pasqualini, E.; Sauphanor, B. Diversity of insecticide resistance mechanisms and spectrum in European populations of codling moth *Cydia pomonella*. *Pest. Manag. Sci.* **2007**, *63*, 890–902.
- (11) Rodríguez, M. A.; Bosch, D.; Sauphanor, B.; Avilla, J. Susceptibility to organophosphate insecticides and activity of detoxifying enzymes in Spanish populations of *Cydia pomonella* (Lepidoptera: Tortricidae). *J. Econ. Entomol.* **2010**, *103*, 482–491.
- (12) Fuentes-Contreras, E.; Reyes, M.; Barros, W.; Sauphanor, B. Evaluation of azinphos-methyl resistance and activity of detoxifying enzymes in codling moth (Lepidoptera: Tortricidae) from central Chile. *J. Econ. Entomol.* **2007**, *100*, 551–556.
- (13) Soleño, J.; Anguiano, L.; D'Angelo, A. P.; Cichón, L.; Fernández, D.; Montagna, C. Toxicological and biochemical response to azinphos-

- methyl in *Cydia pomonella* L. (Lepidoptera: Tortricidae) among orchards from the Argentinian Patagonia. *Pest. Manag. Sci.* **2008**, *64*, 964–970.
- (14) Newcomb, R. D.; Campbell, P. M.; Ollis, D. L.; Cheah, E.; Russell, R. J.; Oakeshott, J. G. A single amino acid substitution converts a carboxylesterase to an organophosphorus hydrolase and confers insecticide resistance on a blowfly. *Proc. Natl. Acad. Sci. U.S.A.* **1997**, *94*, 7464–7468.
- (15) Cui, F.; Lin, Z.; Wang, H.; Liu, S.; Chang, H.; Reeck, G.; Qiao, C.; Raymond, M.; Kang, L. Two single mutations commonly cause qualitative change of nonspecific carboxylesterases in insects. *Insect Biochem. Mol. Biol.* **2011**, *41*, 1–8.
- (16) Claudianos, C.; Russell, R. J.; Oakeshott, J. G. The same amino acid substitution in orthologous esterases confers organophosphate resistance on the house fly and a blowfly. *Insect Biochem. Mol. Biol.* **1999**, *29*, 675–686.
- (17) Bencharit, S.; Morton, C. L.; Howard-Williams, E. L.; Danks, M. K.; Potter, P. M.; Redinbo, M. R. Structural insights into CPT-11 activation by mammalian carboxylesterases. *Nat. Struct. Mol. Biol.* **2002**, *9*, 337–342.
- (18) Bencharit, S.; Edwards, C. C.; Morton, C. L.; Howard-Williams, E. L.; Kuhn, P.; Potter, P. M.; Redinbo, M. R. Multisite promiscuity in the processing of endogenous substrates by human carboxylesterase 1. *J. Mol. Biol.* **2006**, *363*, 201–214.
- (19) Wierdl, M.; Morton, C. L.; Nguyen, N. K.; Redinbo, M. R.; Potter, P. M. Molecular Modeling of CPT-11 Metabolism by Carboxylesterases (CEs): Use of pnb CE as a Model. *Biochemistry* **2004**, *43*, 1874–1882.
- (20) Bourne, Y.; Hasper, A. A.; Chahinian, H.; Juin, M.; Graaff, L. H. d.; Marchot, P. *Aspergillus niger* protein EstA defines a new class of fungal esterases within the α/β hydrolase fold superfamily of proteins. *Structure* **2004**, *12*, 677–687.
- (21) Bencharit, S.; Morton, C. L.; Xue, Y.; Potter, P. M.; Redinbo, M. R. Structural basis of heroin and cocaine metabolism by a promiscuous human drug-processing enzyme. *Nat. Struct. Mol. Biol.* **2003b**, *10*, 345–356.
- (22) Hamza, A.; Cho, H.; Tai, H. H.; Zhan, C. G. Molecular dynamics simulation of cocaine binding with human butyrylcholinesterase and its mutants. *J. Phys. Chem. B* **2005**, *109*, 4776–4782.
- (23) Rose, T. M.; Henikoff, J. G.; Henikoff, S. CODEHOP (Consensus-Degenerate Hybrid Oligonucleotide Primer) PCR primer design. *Nucleic Acids Res.* **2003**, *31*, 3763–3766.
- (24) Rombel, I. T.; Sykes, K. F.; Rayner, S.; Johnston, S. A. ORF-FINDER: a vector for high-throughput gene identification. *Gene* **2002**, *282*, 33–41.
- (25) Tamura, K.; Dudley, J.; Nei, M.; Kumar, S. MEGA4: Molecular evolutionary genetics analysis (MEGA) software version 4.0. *Mol. Biol. Evol.* **2007**, *24*, 1596–1599.
- (26) Bendtsen, J. D.; Nielsen, H.; Heijne, G. V.; Brunak, S. Improved prediction of signal peptides: SignalP 3.0. *J. Mol. Biol.* **2004**, *340*, 783–795.
- (27) Pierleoni, A.; Martelli, P. L.; Casadio, R. PredGPI: a GPI-anchor predictor. *BMC Bioinf.* **2008**, *9*, 392.
- (28) Hansen, J. E.; Lund, O.; Tolstrup, N.; Gooley, A. A.; Williams, K. L.; Brunk, S. NetOglyc: Prediction of mucin type O-glycosylation sites based on sequence context and surface accessibility. *Glycoconjugate J.* **1998**, *15*, 115–130.
- (29) Šali, A.; Blundell, T. L. Comparative protein modelling by satisfaction of spatial restraints. *J. Mol. Biol.* **1993**, *234*, 779–815.
- (30) Thompson, J. D.; Gibson, T. J.; Plewniak, F.; Jeanmougin, F.; Higgins, D. G. The ClustalX windows interface: flexible strategies for multiple sequence alignment aided by quality analysis tools. *Nucleic Acids Res.* **1997**, *25*, 4876–4882.
- (31) Chen, V. B.; Arendall, B. A.; Headd, J. J.; Keedy, D. A.; Immormino, R.; Kapral, G. J.; Murray, L. W.; Richardson, J. S.; Richardson, D. MolProbity: all-atom structure validation for macromolecular crystallography. *Acta Crystallogr.* **2010**, *D66*, 12–21.
- (32) Jones, G.; Willett, P.; Glen, R. C. Molecular recognition of receptor sites using a genetic algorithm with a description of desolvation. *J. Mol. Biol.* **1995**, *245*, 43–53.
- (33) Jones, G.; Willett, P.; Glen, R. C.; Leach, A. R.; Taylor, R. Development and validation of a genetic algorithm for flexible docking. *J. Mol. Biol.* **1997**, *267*, 727–748.
- (34) LePage, J. T.; Hebert, V. R.; Tomaszecka, E. M.; Rothlein, J. E.; McCauley, L. Determination of acephate in human urine. *J. AOAC Int.* **2005**, *88*, 1788–1792.
- (35) Macrae, C. F.; Bruno, I. J.; Chisholm, J. A.; Edgington, P. R.; McCabe, P.; Pidcock, E.; Rodriguez-Monge, R.; Taylor, R.; van de Streek, J.; Wood, P. A. Mercury CSD 2.0-New features for the visualization and investigation of crystal structures. *J. Appl. Crystallogr.* **2008**, *41*, 466–470.
- (36) Korb, O.; Stützle, T.; Exner, T. E. Empirical scoring functions for advanced protein-ligand docking with Plants. *J. Chem. Inf. Model.* **2009**, *49*, 84–96.
- (37) Zhang, Z.; Li, L.; Lin, B.; Schroeder, M.; Huang, B. Identification of cavities on protein surface using multiple computational approaches for drug binding site prediction. *Bioinformatics* **2011**, *27*, 2083–2088.
- (38) DeLano, W. L. *The PyMol Molecular Graphics System*; DeLano Scientific: California, 2010.
- (39) Humphrey, W.; Dalke, A.; Schulten, K. VMD-virtual molecular dynamics. *J. Mol. Graphics. Modell.* **1996**, *14*, 33–38.
- (40) Maestro; Schrodinger Inc.: USA, 2008.
- (41) Case, D. A.; Darden, T. A.; Cheatham, T. E., III; Simmerling, C. L.; Wang, J.; Duke, R. E.; Luo, R.; Walker, R. C.; Zhang, W.; Merz, K. M.; Roberts, B.; Hayik, S.; Roitberg, A.; Seabra, G.; Swails, J.; Goetz, A. W.; Kolossaváry, I.; Wong, K. F.; Paesani, F.; Vanicek, J.; Wolf, R. M.; Liu, J.; Wu, X.; Brozell, S. R.; Steinbrecher, T.; Gohlke, H.; Cai, Q.; Ye, X.; Wang, J.; Hsieh, M. J.; Cui, G.; Roe, D. R.; Mathews, D. H.; Settin, M. G.; Salomon-Ferrer, R.; Sagui, C.; Babin, V.; Luchko, T.; Gusarov, S.; Kovalenko, A.; Kollman, P. A. AMBER 12; University of California: San Francisco, 2012.
- (42) Wang, J.; Wolf, R. M.; Caldwell, J. W.; Kollman, P. A.; Case, D. A. Development and testing of a general amber force field. *J. Comput. Chem.* **2004**, *25*, 1157–1174.
- (43) Jakalian, A.; Jack, D. B.; Bayly, C. Fast, efficient generation of high-quality atomic charges. AM1-BCC model: II. Parameterization and validation. *J. Comput. Chem.* **2002**, *23*, 1623–1641.
- (44) Hummer, G.; Rasaiah, J. C.; Noworyta, J. P. Water conduction through the hydrophobic channel of a carbon nanotube. *Nat. Struct. Mol. Biol.* **2001**, *414*, 188–190.
- (45) Berendsen, H. J. C.; Postma, J. P. M.; Gunsteren, W. F. V.; DiNola, A.; Haak, J. R. Molecular dynamics with coupling to an external bath. *J. Chem. Phys.* **1984**, *81*, 3684–3690.
- (46) Ryckaert, J. P.; Cicotti, G.; Berendsen, H. J. C. Numerical integration of the Cartesian equations of motion of a system with constraints: molecular dynamics of *n*-alkanes. *J. Comput. Phys.* **1977**, *23*, 327–341.
- (47) Essmann, U.; Perera, L.; Berkowitz, M. L.; Darden, T.; Lee, H.; Pedersen, L. G. A smooth particle mesh Ewald method. *J. Chem. Phys.* **1995**, *103*, 8577–8593.
- (48) Kollman, P. A.; Massova, I.; Reyes, C.; Kuhn, B.; Huo, S.; Chong, L.; Lee, M.; Lee, T.; Duan, Y.; Wang, W.; Donini, O.; Cieplak, P.; Srivivasan, J.; Case, D. A.; Cheatham, T. E. Calculating structures and free energies of complex molecules: combining molecular mechanics and continuum models. *Acc. Chem. Res.* **2000**, *33*, 889–897.
- (49) Wang, H.; Hou, T.; Xu, X. Recent advances in free energy calculations with a combination of molecular mechanics and continuum models. *Curr. Comput.-Aided Drug Des.* **2006**, *2*, 287–306.
- (50) Hou, T.; Wang, J.; Li, Y.; Wang, W. Assessing the performance of the MM/PBSA and MM/GBSA methods. I. The accuracy of binding free energy calculations based on molecular dynamics simulations. *J. Chem. Inf. Model.* **2011**, *51*, 69–82.
- (51) Hou, T.; Wang, J.; Li, Y.; Wang, W. Assessing the performance of the molecular mechanics/Poisson Boltzmann surface area and molecular mechanics/generalized Born surface area methods. II. The

- accuracy of ranking poses generated from docking. *J. Comput. Chem.* **2011**, *32*, 866–877.
- (52) Weiser, J.; Shenkin, P. S.; Still, W. C. Approximate atomic surfaces from linear combinations of pairwise overlaps (LCPO). *J. Comput. Chem.* **1999**, *20*, 217–230.
- (53) Hou, T. J.; Zhang, W.; Case, D. A.; Wang, W. Characterization of domain-peptide interaction interface: a case study on the amphiphysin-1 SH3 domain. *J. Mol. Biol.* **2008**, *376*, 1201–1214.
- (54) Gohlke, H.; Kiel, C.; Case, D. A. Insights into protein-protein binding by binding free energy calculation and free energy decomposition for the Ras-Raf and Ras-RalGDS complexes. *J. Mol. Biol.* **2003**, *330*, 891–913.
- (55) Moreira, I. S.; Fernandes, P. A.; Ramos, M. J. Computational alanine scanning mutagenesis-An improved methodological approach. *J. Comput. Chem.* **2007**, *28*, 644–654.
- (56) Huo, S.; Massova, I.; Kollman, P. A. Computational alanine scanning of the 1:1 human growth hormone-receptor complex. *J. Comput. Chem.* **2002**, *23*, 15–27.
- (57) Massova, I. S.; Kollman, P. A. Computational alanine scanning to probe protein-protein interactions: a novel approach to evaluate binding free energies. *J. Am. Chem. Soc.* **1999**, *121*, 8133–8143.
- (58) Yang, X. Q.; Zhang, Y. L. Effect of temperature and sorbitol in improving the solubility of carboxylesterases protein CpCE-1 from *Cydia pomonella* and biochemical characterization. *Appl. Microbiol. Biotechnol.* **2013**, *97*, 10423–10433.
- (59) Bradford, M. M. A rapid and sensitive method for the quantitation of microgram quantities of protein utilizing the principle of protein-dye binding. *Anal. Biochem.* **1976**, *72*, 248–254.
- (60) Hamilton, M. A.; Russo, R. C.; Thurston, R. V. Trimmed Spearman-Karber method for estimating median lethal concentration in toxicity bioassays. *Environ. Sci. Technol.* **1977**, *11*, 714–719.
- (61) Cer, R. Z.; Mudunuri, U.; Stephens, R.; Lebeda, F. J. *IC₅₀*-to-*K_i*: a web-based tool for converting *IC₅₀* to *K_i* values for inhibitors of enzyme activity and ligand binding. *Nucleic Acids Res.* **2009**, *37*, 441–445.
- (62) Bowie, J. U.; Lüthy, R.; Eisenberg, D. A method to identify protein sequences that fold into a known three-dimensional structure. *Science* **1991**, *253*, 164–170.
- (63) Lüthy, R.; Bowie, J. U.; Eisenberg, D. Assessment of protein models with three-dimensional profiles. *Nature* **1992**, *356*, 83–85.
- (64) Dundas, J.; Ouyang, Z.; Tseng, J.; Binkowski, A.; Turpaz, Y.; Liang, J. CASTp: computed atlas of surface topography of proteins with structural and topographical mapping of functionally annotated residues. *Nucleic Acids Res.* **2006**, *34*, W116–W118.
- (65) Song, X.; Gragen, S.; Li, Y.; Ma, Y.; Liu, J.; Yang, D.; Matoney, L.; Yan, B. Intramolecular disulfide bonds are required for folding hydrolase B into a catalytically active conformation but not for maintaining it during catalysis. *Biochem. Biophys. Res. Co.* **2004**, *319*, 1072–1080.
- (66) Pan, P. C.; Li, Y. Y.; Yu, H. D.; Sun, H. Y.; Hou, T. J. Molecular principle of topotecan resistance by topoisomerase I mutations through molecular modeling approaches. *J. Chem. Inf. Model.* **2013**, *53*, 997–1006.
- (67) Cui, F.; Qu, H.; Cong, J.; Liu, X. L.; Qiao, C. L. Do mosquitoes acquire organophosphate resistance by functional changes in carboxylesterases? *FASEB J.* **2007**, *21*, 3584–3591.
- (68) Zhu, X. L.; Yang, W. C.; Yu, N. Y.; Yang, S. G.; Yang, G. F. Computational simulations of structural role of the active-site W374C mutation of acetyl-coenzyme-A carboxylase: Multi-drug resistance mechanism. *J. Mol. Model.* **2011**, *17*, 495–503.
- (69) Coppin, C. W.; Jackson, C. J.; Sutherland, T.; Hart, P. J.; Devonshire, A. L.; Russell, R.; Oakeshott, J. G. Testing the evolvability of an insect carboxylesterase for the detoxification of synthetic pyrethroid insecticides. *Insect Biochem. Mol. Biol.* **2012**, *42*, 343–352.
- (70) Joerger, A. C.; Ang, H. C.; Fersht, A. R. Structural basis for understanding oncogenic p53 mutations and designing rescue drugs. *Proc. Natl. Acad. Sci. U.S.A.* **2006**, *103*, 15056–15061.
- (71) Zhu, X. L.; Ge, F. H.; Zhan, C. G.; Yang, G. F. Computational simulations of the interactions between acetyl-coenzyme-A carboxylase and clodinafop resistance mechanism due to active and nonactive site mutations. *J. Chem. Inf. Model.* **2009**, *49*, 1936–1943.
- (72) Morin, A.; Meiler, J.; Mizoue, L. S. Computational design of protein-ligand interfaces: potential in therapeutic development. *Trends Biotechnol.* **2011**, *29*, 159–166.
- (73) Cao, Z. W.; Han, L. Y.; Zheng, C. J.; Ji, Z. L.; Chen, X.; Lin, H. H.; Chen, Y. Z. Computer prediction of drug resistance mutations in proteins. *Drug Discovery Today* **2005**, *10*, 521–529.
- (74) Hollomon, D. Do we have the tools to manage resistance in the future? *Pest Manag. Sci.* **2012**, *68*, 149–154.
- (75) Bouvier, J. C.; Buès, R.; Boivin, T.; Boudinon, L.; Beslay, D.; Sauphanor, B. Deltamethrin resistance in the codling moth (Lepidoptera: Tortricidae): inheritance and number of genes involved. *Heredity* **2001**, *87*, 456–462.
- (76) Kuchner, O.; Arnold, F. H. Directed evolution of enzyme catalysts. *Trends Biotechnol.* **1997**, *15*, 523–530.
- (77) Chen, R. Enzyme engineering: rational redesign versus directed evolution. *Trends Biotechnol.* **2001**, *19*, 13–14.
- (78) Argiridi, M. A.; Goedken, E. R.; Banach, D.; Borhani, D. W.; Burchat, A.; Dixon, R. W.; Marcotte, D.; Overmeyer, G.; Pivorunas, V.; Sadhukhan, R.; Sousas, S.; Moore, N. S. J.; Tomlinson, M.; Voss, J.; Wang, L.; Wishart, N.; Woller, K.; Talanian, R. V. Enabling structure-based drug design of Tyk2 through co-crystallization with a stabilizing aminoindazole inhibitor. *BMC Struct. Biol.* **2012**, *12*, 1–11.